Future of Satellite Reentry and Earth's Atmosphere: the Lifetime and Direct Radiative Forcing of Space Debris Reentry Alumina

Asha K. Jain [1], Sebastian D. Eastham [1,2], Daniel E. Hastings [1]

[1]MIT Department of Aeronautics and Astronautics
[2]Joint Program on the Science and Policy of Global Change, Center for Global Change Science, Massachusetts Institute of Technology

Key Points:

- Reentry-ablated alumina has a 1 to 2 year lifetime and produces a cooling direct radiative forcing of approximately -0.4 to -0.5 mW/m^2.
- Assuming a constant flux of alumina, rather than resolving each reentry event, results in a 22% larger radiative cooling.
- These results are sensitive to uncertainties on the characteristics and behavior of reentry-ablated alumina which warrant future work.

Corresponding author: Sebastian Eastham, `seastham@mit.edu`

Abstract

Numerous satellite operators are building megaconstellations in Low Earth Orbit (LEO) with hundreds of satellites, placing new satellites and spent rocket stages in orbit. Once these objects fail, they are often removed from LEO via atmospheric reentry, producing metallic particles that can interact with ozone chemistry and Earth's radiative balance. The extent of these interactions remains poorly understood despite their importance to current space governance and policymaking.

Helping to address this gap, this paper estimates the distribution, lifetime and direct radiative forcing of reentry-ablated alumina using an Earth system model. We consider a future scenario where all megaconstellations publicly filed at the Federal Communications Commission as of 2022 are operating, amounting to 2.52 Gg/yr of reentry-ablated alumina emissions. As a conservative approximation, we find that reentry-ablated alumina particles have an atmospheric lifetime between one and two years, leading to a cooling radiative forcing of approximately -0.378 mW/m^2. Simulations with fine alumina particles produce between 14% and 36% larger radiative forcings and have lifetimes 1.54 times longer than simulations with coarse alumina emissions. Alumina emitted only in the South Pacific produces an asymmetrical radiative forcing. Furthermore, modeling alumina with time-averaged, constant emissions rather than in discrete reentry plumes in results in 21% to 24% overestimation of alumina's radiative forcing.

These results are sensitive to numerous assumptions on initial particle size, radiative indices and coagulation characteristics of the aerosol. In-situ observation and a sophisticated understanding of reentry-ablated alumina particles are necessary to better predict the atmospheric consequences of reentry-ablated alumina.

Plain Language Summary

The number of satellites and spent rocket stages reentering into Earth's atmosphere is increasing. The development of megaconstellations, or systems with hundreds of satellites, is contributing to this rise in reentry. These systems necessitate numerous launches to build out and maintain the constellation size, leading to consistent insertions of new satellites and rocket bodies into orbit, and similarly, repetitive reentries of dead objects into Earth's atmosphere. During reentry, these objects experience extreme heating that causes parts to melt into small metallic particles.

These particles are left behind in atmosphere at high altitudes where they accumulate and interact with important atmospheric processes, including ozone depletion and global warming. This work aims to estimate the climate implications of alumina particles formed during space debris reentry. Using a state-of-the-art atmospheric model, we create reentry emissions that correspond to 13,900 satellite and 500 rocket stage reentries per year, or 2.52 Gg/yr of alumina.

We find that these particles persist 1 to 2 years in the atmosphere and cause a global cooling effect. These results help characterize the atmospheric consequences of long-term, repetitive emissions of alumina particles at high altitudes and show that further study and monitoring of these emissions is justified.

1 Introduction

Space debris reentry into Earth's atmosphere is becoming more frequent due to the growing number of objects in Low Earth Orbit (LEO) which rely on reentry for disposal (European Space Agency, 2022a). Between 2020 and 2022, the number of reentries more than doubled from 93 to 197 per year, hitting a new decadal high (Center for Orbital and Reentry Debris Studies, 2023). Traveling at near orbital velocity, space debris reen-

tries ablate in the upper atmosphere, producing reentry by-products that can interact with important upper atmospheric processes. Despite rising reentry rates, the scope and severity of these atmospheric interactions are poorly understood. Helping to address this gap, this article presents estimations for distribution, lifetime and instantaneous radiative forcing of reentry-ablated alumina. We also study the sensitivity of these results to different representations of alumina emissions, varying the initial particle size distribution, emission location, and resolution of individual reentry events.

As of 2023, there are more than 20,000 objects tracked in LEO which is double the 2013 LEO population (European Space Agency, 2022a). Megaconstellations, or groups of hundreds to tens of thousands of satellites that work together to provide a service, are responsible in large part for this growth (Ryan-Mosley et al., 2019; Rainbow, 2022). These systems require numerous launches to deploy and maintain, leading to a stream of new satellites and spent rocket stages into LEO (Ryan-Mosley et al., 2019; Rainbow, 2022). As governments, space agencies, and commercial operators work to manage this space traffic, atmospheric reentry is often recommended for Low Earth to geostationary transfer orbits to remove unwanted, defunct objects (United Nations, 2019). Several policies also impose mandatory deadlines for disposing of space objects (Federal Communications Commission, 2022a). As a result of growing space activity and requirements to deorbit, the number of atmospheric reentries is expected to rise over the next decade. Some projections estimate that megaconstellations could account for approximately 78,000 satellites orbiting in LEO when fully developed (Williams et al., 2021). Assuming a common LEO satellite lifetime of 5 years for each of these satellites, this orbital population would generate a steady state reentry flux of 15,600 satellites per year—two orders of magnitude larger than the present day reentry flux of approximately 200 reentries per year (Center for Orbital and Reentry Debris Studies, 2023).

Recognizing the potential for environmental consequences, regulators, corporations and aerospace consumers are gaining interest in understanding the atmospheric salience of space debris reentries (Jones et al., 2023). In late 2022, the Federal Communication Commission (FCC) added provisions to a megaconstellation license to conduct environmental studies on reentry-ablated alumina (Federal Communications Commission, 2022b). Since regulators must decide at present whether to approve megaconstellations with potential future environmental consequences, there is a need to understand the impact of long-term, repetitive space debris reentries at proposed future reentry rates. Furthermore, making this kind of analysis accessible and comparable to other industries is critical for informed regulations and decisionmaking. Thus, in this work, we estimate the instantaneous radiative forcing, a common metric used to understand the global climate impact in several industries (Ross & Sheaffer, 2014; Lee et al., 2021).

1.1 Brief Overview of Atmospheric Reentry

Space debris reentries can achieve surface temperatures over 900°K at altitudes between 90 km and 30 km while flying 1000 km to 1500 km downrange (Ziniu et al., 2011; Lips, 2003). Aluminum, a common space debris material, rapidly melts at these temperatures (Greene & Sanchez, 2019). Aerodynamic shear over molten aluminum leads to particle spraying which is the dominant mode of mass loss for aluminum components (Greene & Sanchez, 2019). Nearly all of this reentry-ablated aluminum is predicted to oxidize into alumina (Al_2O_3), creating a source of high-altitude alumina particle emissions (Park & Park, 2017).

Moreover, the current influx of space debris aluminum is likely outpacing the meteoric aluminum influx by 130 to 340 percent and growing (Jain & Hastings, 2022). This difference in the amount of man-made versus natural aluminum emissions could allow anthropogenic reentries to meaningfully alter the composition and consequently, behavior of the upper atmosphere (Jain & Hastings, 2022; Schulz & Glassmeier, 2021).

At present, the physical, optical and chemical characteristics of reentry-ablated alumina are understudied. The violent nature of reentry and difficulties reproducing reentry-like conditions on Earth present challenges to capturing reentry-ablated particles for later analysis. While there have been some arc-jet studies on the demisability of aluminum, these studies did not attempt to capture nor characterize the ablated aluminum particles (Beck et al., 2019; Greene & Sanchez, 2019). Furthermore, observations of reentry events are sparse and predicting reentry location is extremely difficult, making it hard to estimate where reentry emissions occur for in-situ sampling (Pardini & Anselmo, 2008; Anwar, 2022). Given these uncertainties, we assess the sensitivity of our results to different particle size distributions and reentry locations.

1.2 Impact of High Altitude Emissions

Reentry models have shown that space debris reentries release alumina particles between 30 km and 85 km, far above commercial aviation emissions at 8 km to 12 km (Bekki et al., 2021). At these altitudes, emissions can have longer atmospheric lifetimes than tropospheric or surface emissions, increasing their influence on atmospheric processes. For example, rocket exhaust particles can persist for 3-5 years in the stratosphere, while particles from aviation jet exhaust in the upper troposphere only remain suspended for several months (Wilcox et al., 2012; Waugh & Hall, 2002). Compounding their impact, upper atmospheric emissions can directly interact with the ozone layer which is thickest between 15 km to 40 km (US EPA, OAR, 2017). Studies on stratospheric supersonic transport have shown that the impact of NO_x on ozone depletion and radiative forcing strongly increases with altitude above 17 km (Zhang et al., 2021; Fritz et al., 2022). The coupled effects of longer atmospheric lifetimes and direct emission into the ozone layer make the high-altitude emissions from space debris reentries of particular interest.

Given the long term consequences of high altitude emissions, several studies have estimated the consequences of rocket launches and reentries on ozone depletion and radiative forcing. The European Space Agency (ESA) sponsored two studies to explore space debris reentry impacts on stratospheric ozone concentrations and certain radiative forcing mechanisms (European Space Agency, 2022b; Bekki et al., 2021; Bianchi et al., 2021). These studies present limited information on the methodology, assumptions and modeling uncertainty. From publicly available documents, Bekki et al. (2021) presented results that indicate reentry NO_x causes minimal ozone depletion with the most potent effects at high altitudes over Antarctica. This study also found that the radiative forcing from 20 years of consistent levels of reentries was insignificant. Similarly, Bianchi et al. (2021) investigated the effects of a single reentry and yearly reentries on ozone depletion and radiative forcing and found negligible changes. However, the direct radiative effect of alumina particles were neglected in both studies, and only the indirect radiative effect from ozone depletion was quantified (European Space Agency, 2022b).

Modeling modern rocket fleets, Ross and Sheaffer (2014) found that rocket-emitted CO_2, H_2O, black carbon, and alumina produces a direct radiative forcing of approximately 16 mW/m^2. Black carbon accounted for 70% of this rocket forcing while alumina accounted for 28%. With the caveat of poorly constrained aerosol microphysics, this study found that alumina has a net positive radiative forcing, absorbing more outgoing terrestrial longwave radiation than scattering incoming solar radiation (Ross & Sheaffer, 2014). This result is contrary to findings from geoengineering studies of stratospheric alumina. Weisenstein et al. (2015) found that 4 Tg/yr of 240 nm alumina emitted in the stratosphere results in a cooling radiative forcing of -1.2 W/m^2. This difference in findings highlights the importance of an improved understanding of the optical properties and atmospheric behavior of reentry-ablated alumina.

Unlike reentry emissions which predominately occur above 40 km, Ross and Sheaffer (2014) and Weisenstein et al. (2015) only considered alumina emissions in the strato-

sphere between 10 and 40 km. The behavior of alumina emitted in the mesosphere from reentries has yet to be explored. We address this gap in this work, emitting space debris alumina at altitudes between 85 km and 30 km.

In sum, we perform a series of simulations to capture the lifetime, distribution and direct radiative forcing of reentry alumina emissions. We explore the sensitivity of these results to various assumptions on reentry emissions, including the initial particle size distribution and the emission location. We also consider how resolving individual reentry events rather than using time-averaged emissions alters our findings. Finally, we compute the Global Warming Potential over a 20 year horizon and compare our results with similar estimations for the aviation and rocket industries.

2 Methods

We characterize the steady-state behavior of space debris alumina emissions to identify the long term consequences of a specific reentry alumina influx. This approach best represents the steady state operation of fully-developed megaconstellations that maintain a constant orbital population and satellite lifetime, leading to a constant reentry flux.

2.1 Representing Reentry Emissions

This work uses a forecast of the satellite and rocket body orbital population to estimate the future number of reentries. This forecast is based on an economically optimistic future where all of the megaconstellations publicly filed at the Federal Communications Commission as of 2022 achieve their stated design constellation size. This hypothetical scenario corresponds to a yearly reentry flux of 13,900 satellites and 500 rocket bodies, resulting in one reentry occurring approximately every 40 mins (Jones et al., 2023). Satellites are assumed to have an average dry mass of 600 kg while rocket bodies are assumed to have an average dry mass of 2,800 kg (Jones et al., 2023).

We assume that satellites are 21% aluminium while rocket bodies are 70% aluminum (Jain & Hastings, 2022). We also assume an ablation-over-altitude profile that results in approximately 59% and 31% of satellite and rocket body aluminum ablating respectively (Jain & Hastings, 2022). We assume that each pair of aluminum atoms oxidizes into alumina. With these assumptions, our reentry scenario results in 2.52 Gg of emitted alumina per year.

Each reentry is modeled as a discrete event with respect to time and space such that there are numerous impulse emissions in a year distributed across the atmosphere. Due to the default timestep in our high-top Earth system model, these impulse emissions occur for 30mins even though an average reentry last less than 5mins (Lips, 2003). This approach contrasts with other modeling techniques which are commonly used in meteor atmospheric modeling that assume a constant distribution of emissions over a latitude, altitude and longitude band (Plane et al., 2021, 2015). We explore the sensitivity of our results across these two modeling techniques.

The latitude and longitude for each emission is sampled from an equal-area histogram binning of the positions of reentry objects during the last phases of reentry. These groundtracks are generated from the 1969 to 2022 reentry population. Using Two-Line Element (TLE) data and the Simplified General Perturbations-4 (SPG4) orbital propagator, we compute the groundtrack locations at minute intervals, and exclude locations with an altitude greater than 120 km. This groundtrack histogram has a gradually increasing probability of reentry from the equator to higher latitudes until approximately 50 degrees. Above this latitude, the probability of reentry falls. The Northern Hemisphere has slightly higher chances of reentry than the Southern Hemisphere due to a number of inclined,

elliptical reentry objects which had apogees above 120 km in the Southern Hemisphere, resulting in the exclusion of those groundtrack locations. Figure 1 shows the randomly sampled reentry locations for all reentry events in a single emission year using a 0.9°× 1.25° grid.

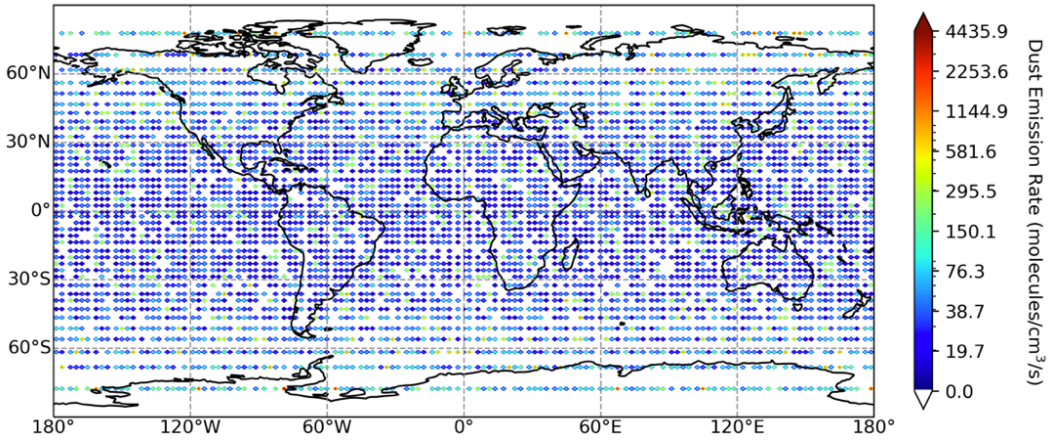

Figure 1: Time-Averaged Spatial Histogram of Reentry-ablated Alumina Plume Emissions into WACCM atmospheric grid volumes at 59-61 km (2 km grid depth). Locations with larger emission concentrations are either the site of multiple emissions over time, or had more massive reentry objects (ie rocket body, rather than satellite reentries). WACCM grid volumes are computed from the grid area multiplied by the grid depth, which is 2 km in this case. Grid areas for a 0.9° × 1.25° grid can be found at repository created by Mills (2022).

,

2.2 Atmospheric Model Selection and Setup

The Whole Atmosphere Community Climate Model (WACCM) is a high-top general circulation model with a model top of approximately 140 km (Marsh et al., 2013). WACCM works with the NCAR Community Earth System Model (CESM) which integrates individual component models for the atmosphere, land, land ice, river runoff, ocean, wave and sea ice interactions. In this work, only the atmosphere and land models are interactive while the rest of these component models are data-driven. Here, interactive implies that each iteration of the model is computed through an evaluation of physical equations, whereas data-driven models read in values for the subsequent timesteps.

Since this study aims to characterize the radiative forcing of reentry alumina, we employ the specified chemistry version of WACCM (WACCM6-SC) with fixed sea surface temperature from year 2000 data. Despite its limited chemistry, WACCM-SC produces nearly identical climatology, and variability of the stratosphere, troposphere and surface climate when compared to full chemistry, free-running WACCM6 experiments (Smith et al., 2014). In this work, climatology from year 2000 is repeated identically year-over-year. We also selected a 0.9°×1.25° degree atmospheric grid with 70 pressure levels.

WACCM6-SC uses the Modal Aerosol Model with four aerosol modes (MAM4) to model dust, sea salt, primary organic matter, black carbon and sulfate aerosols (Liu et al., 2016). These aerosols are grouped into the model's four modes (Aitken, accumulation, coarse and primary carbon) and are assumed to be internally mixed with prede-

Table 1: Aerosol Mode Definitions in CAM6 - MAM4 and Dust (Ke et al., 2022; Liu et al., 2012; Liu, 2023)

Aerosol Mode	Minimum Radius (μm)	Maximum Radius (μm)	Geometric Standard Deviation	Dust Mass-Weighted Diameter (μm)
Aitken	0.01	0.1	1.6	0.0887
Accumulation	0.1	1	1.6	0.781
Coarse	1	10	1.2	3.90

termined, lognormal size distributions (Liu et al., 2016). Particles can coagulate within and across modes, and transition into larger modes. All aerosols are radiatively active, although only some participate in heterogeneous chemistry.

Radiatively active species and aerosols in WACCM6-SC are prescribed in the stratosphere and troposphere with the exception of terrestrial dust (Gettelman et al., 2019). However, cloud formation and its subsequent radiative forcing are computed interactively. The Rapid Radiative Transfer Model for General Circulation Models (GCM)s, termed RRTM-G is used to compute the radiative fluxes at the surface, across the tropopause and at the top of the atmosphere (Iacono et al., 2008; Mlawer et al., 1997; Iacono et al., 2000; Clough et al., 2005).

One limitation of WACCM6-SC is that shortwave heating is prescribed above 65 km (Smith et al., 2014). This approach will obscure any shortwave radiative effects of user-specified emissions above 65 km. Our results show that the majority of the emitted reentry alumina quickly descends below 65 km with peak accumulation in the lower stratosphere. As a result, the majority of the reentry alumina mass will contribute to active radiative calculations, although this limitation in our methodology should be refined for a higher fidelity results.

2.3 Dust as a Proxy for Alumina

Since MAM4 does not directly support alumina aerosol modeling, we use terrestrial mineral dust ($AlSiO_5$) as a proxy. Dust can exist in the Aitken, accumulation and coarse modes, shown in Table 1 (Ke et al., 2022; Liu et al., 2012; Liu, 2023). We use the mass-weighted diameter and an assumption of spherical particles to compute aerosol number emissions, paralleling the procedure used for terrestrial dust emissions (Liu, 2023; Liu et al., 2016). This approach results in particles with initial sizes near the center of each mode's lognormal distribution.

No modifications to the dust size distributions are made to test additional particle size distributions for reentry-ablated alumina. Any modifications to the dust properties would alter the surface dust emissions, leading to potential error in the terrestrial dust behavior and lifetime in the troposphere. This error may cause unreasonable atmospheric behavior and unrealistic model results. For this reason, no physical nor optical properties of dust are modified to better mimic alumina. For reference, terrestrial dust coagulates within and across aerosol modes, has a hygroscopicity of 0.06, and undergoes wet and dry deposition in WACCM. This approach differs slightly from a geoengineering study of alumina which assumed spherical alumina particles are hydrophobic until coated in sulfate Weisenstein et al. (2015).

Like alumina, dust is radiatively active in WACCM6. RRTMG uses the refractive indices of an aerosol over several bands of wavelengths to compute the single scattering

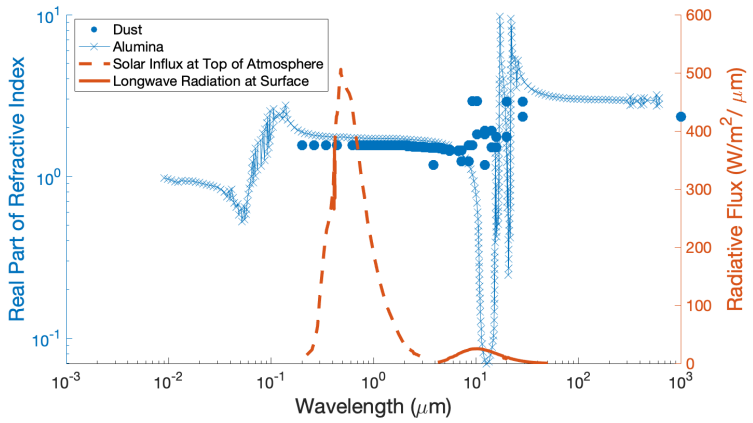

(a) Real Part of Refractive Indices

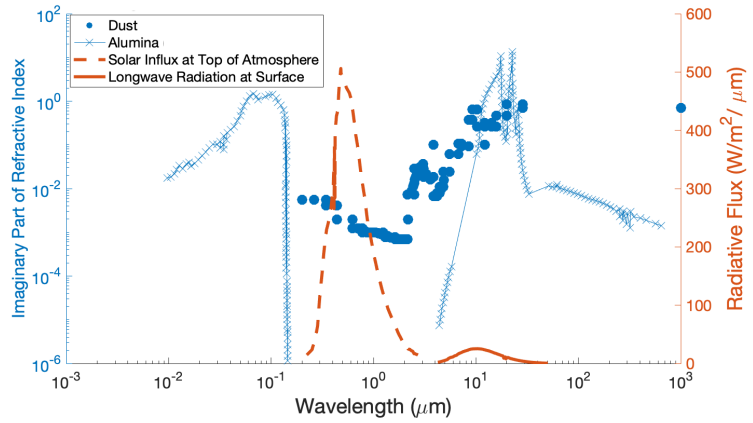

(b) Imaginary Part of Refractive Indices

Figure 2: Refractive Indices of Terrestrial Dust ($AlSiO_5$) taken from WACCM-RRTMG and Alumina (Al_2O_3) taken from (Palik, 1985) compared to the Solar Influx and Earth's Outgoing Longwave Radiation (taken from (Kiehl & Trenberth, 1997))

albedo (Tilmes et al., 2023; Jo et al., 2017). The refractive indices for alumina and dust are shown in Figure 2, assuming a sign convention of $\bar{n} = n + i\kappa$ where n is the real part and κ is the absorption coefficient.

As Figure 2a shows, the real part of dust and alumina refractive indices are very similar over a number of wavelengths, including over the solar irradiance band. In this region, dust has real refractive indices within 10% error of alumina. At the largest wavelengths, dust underestimates alumina's real refractive index by approximately 20%. Over band of wavelengths of Earth's outgoing radiation, alumina is more transparent than dust. Comparing the absorption coefficients, dust overestimates alumina's absorptivity in short wavelengths, but is a good proxy for long wavelengths, above 100 microns. Overall, terrestrial dust represents a first order approximation of alumina.

2.4 Achieving a Sufficient Signal-to-Noise Ratio

Surface dust emissions in WACCM-SC default to dynamic, online calculations, responding to changing wind patterns and precipitation levels. Since the model's meteorology is not prescribed in WACCM-SC, it is possible that chaotic meteorological feedbacks could drive changes in the surface dust emissions which exceed the our reentry emissions, consequently obscuring the reentry emissions in the stratosphere and troposphere.

Early results confirmed that the surface dust emission variance obscured the reentry "dust" emissions in the stratosphere and troposphere. Motivated by these results, we implement additional modifications to WACCM6-SC to control the surface dust flux. We zero-out prognostic dust calculations and instead prescribe the surface dust flux based on the first year of WACCM-SC prognostic dust emissions. These emissions are repeated identically year-over-year. Unfortunately, WACCM6-SC does not support prescribed meteorology in the troposphere, so this approach decouples the natural feedback between surface dust flux and meteorology. We assume that this error is negligible and limited to the troposphere over short time scales.

In addition to controlling the surface dust flux, we also scaled the reentry alumina flux by a factor of 530 such that the reentry "dust" could be resolved throughout the stratosphere. As a result, each test case emits 1.33 Tg rather than 2.52 Gg of reentry alumina, as estimated from our reentry scenario. We take this higher reentry alumina mass as the emitted dust mass for each case. This approach leads to slightly higher number emissions since terrestrial dust has a lower density than alumina.

We assume a linear relationship between the emitted mass and the radiative effects of reentry "dust" to rescale our results back to our reentry scenario. Several studies on atmospheric aerosols have used this approach to improve signal-to-noise ratios in their respective atmospheric models (Chung, 2005; Miller et al., 2004; Haywood & Shine, 1995, 1995).

2.5 Test Cases

We ran several test cases to analyze the sensitivity of our results to a number of assumptions (see Table 2). We define a small and medium particle case which use the Aitken and accumulation mode for reentry emissions, respectively, to explore the effect of different initial aerosol size distributions. The small and medium particle cases use globally-distributed emissions with a discrete representation for each reentry event. In contrast, we define an averaged case that uses time-averaged emissions to understand the effect of modeling reentries as discrete events. In this averaged case, reentry alumina is emitted in the accumulation mode across the globe, but the discrete representation of reentry plumes is replaced by time-constant emissions with each grid volume emitting its yearly-averaged emitted mass. Finally, we constructed a South Pacific case with discrete reentry emissions in the accumulation mode to test the effect of concentrating all reentries in South Pacific region bounded by 70°S to 10°S and 140°W to 70°W. Due to its relative isolation, the South Pacific has been the site of at least 263 intentional space debris reentries since 1971 to minimize harm to human life and property (De Lucia & Iavicoli, 2019). With this test case, we aim to understand whether concentrating reentries in this location is a sustainable and recommendable practice.

2.6 Post-processing Methods

Using terrestrial dust as a proxy for alumina presents a challenge to isolate the reentry signal, especially in the troposphere where terrestrial dust largely resides. To address this issue, we compute the subset of pressure levels at which the reentry signal is resolvable. A control case with no reentry emissions was used to identify the nominal dust burden at each pressure level. For each perturbed case with reentry emissions, we compare

Table 2: Test Cases

Test Name	Emission Size Mode	Description	Sensitivity Explored
Base	None	Control Case	N/A
Medium Particles	Accumulation	Emissions are discrete events that occur over globe.	Emitted Particle Size
Small Particles	Aikten	Emissions are discrete events that occur over globe.	Emitted Particle Size
Averaged	Accumulation	Time-averaged emissions with constant forcing over time.	Importance of Modeling Discrete Reentry Plumes
South Pacific	Accumulation	Emissions are discrete events that occur only in the South Pacific.	Emission Location

the magnitude of the dust burden at each pressure level with the control case over time. Any pressure level where the burden in the perturbed case is at least one magnitude larger than the control case is considered a part of the pressure level subset that defines the reentry signal. This approach ensures that the perturbed dust mass is at least one order of magnitude larger than the background dust mass which is sufficient to resolve the reentry signal. Every dust mode in all tests cases demonstrated a resolvable reentry signal (hereafter referred to as reentry alumina) from the tropopause to the model top.

For each test case, we also compute the direct radiative forcing of reentry alumina using Equation 1 where F^d indicates radiative fluxes computed with radiatively active dust, N_i indicates the total number of latitude divisions, N_j indicates the total number of longitude divisions, and A_t indicates Earth's total surface area.

$$\text{Direct Radiative Forcing} = \sum_{i=1}^{N_i}\sum_{j=1}^{N_j}[(F^d_{\text{perturbed}} - F_{\text{perturbed}}) - (F^d_{\text{control}} - F_{\text{control}})]\frac{A_{i,j}}{A_t} \tag{1}$$

This approach assumes that the terrestrial dust burden, and consequently, its contribution to radiative forcing, is constant across the perturbed and control case. In practice, the difference in meteorology between the two cases implies that terrestrial dust may be advected differently, resulting in different distributions, burdens and contributions to radiative transfer. However, we find that the difference is not sufficient to obscure direct radiative forcing signal from reentry alumina.

3 Results

3.1 Distribution and Lifetime of Reentry Alumina

The steady state burden and lifetime of reentry alumina are averaged over a two year period from 2002 to 2004, as shown in Table 3. The lifetime of reentry alumina is computed using the burden summed across all dust modes.

We can see several differences in how reentry alumina behaved across the four test cases. First, reentry alumina in the medium particles case coagulates from the accumulation mode to the coarse mode. However, in the small particles case, the emitted Aitken mode particles coagulate into accumulation mode particles which do not readily tran-

Table 3: Steady State Burden and Lifetimes of Reentry Alumina for Every Test Case

Test Case	Aitken (Gg)	Accumulation (Gg)	Coarse (Gg)	Lifetime (days)
Medium Particles	N/A	2.95	1780	487
Small Particles	154	2600	1.37	749
Averaged	N/A	14.8	2100	605
South Pacific	N/A	3.73	1770	485

sition into the coarse mode as it did in the medium particles case. One explanation for this difference is that Aitken mode particles in the small particles case readily collides other particles while in the reentry plume, but as the plume disperses, the resultant accumulation mode particles do not quickly interact with other particles to grow into the coarse mode.

Furthermore, accumulation mode particles in the averaged emissions case maintains a higher steady state burden than in the medium particles which indicates that accumulation mode particles in the averaged emissions case are transitioning into the coarse mode less efficiently. This difference is driven by the time-averaged emissions compared to the discrete reentry event emissions in the medium particles case. Reentry alumina is coagulating efficiently in reentry plumes which is not well captured by a time-constant representation of the same emitted mass. We find further evidence of this phenomena when comparing the coarse mode burden with the accumulation mode burden over short time scales in both cases. This analysis show after a 5 day period, reentry-resolved emissions in the medium particle mode are coagulating into coarse mode particles within 5 days of emission, unlike particles in the averaged case.

The small particles case achieved the longest lifetime at 749 days with majority of the reentry alumina persisting in the accumulation mode. In general, accumulation mode particles tend to be less effective at coagulation compared to smaller particles and coarse mode particles tend to more efficiently nucleate into clouds or deposit on the surface (Liu et al., 2005). Therefore, it follows that the case with the most reentry alumina persisting in the accumulation mode has the longest lifetime. Following similar reasoning, the averaged emission case has the second longest lifetime of 604.7 days. The time-averaged emissions cause slower coagulation and thus slower transitioning from the accumulation to the coarse mode than the medium particles case, resulting in a higher accumulation mode steady state burden. In fact, the averaged emissions case has an order of magnitude more accumulation mode particles than the medium particles case. This result indicates that modeling reentry events as discrete emissions with reentry plumes plays an important role in characterizing the lifetime of reentry alumina. The medium particles case results in a lifetime that is 20% shorter than the averaged emission case, despite having emissions in the same particle size mode.

Despite the concentration of emissions in the southern hemisphere, the South Pacific case shows that the reentry alumina lifetimes are similar to the medium particles case which had global emissions in the same mode. This finding suggests that the reentry alumina lifetime is less sensitive to reentry location than the emitted particle size.

Figure 3 shows zonal distribution of the dominant dust mode in each case. Each zonal distribution was averaged over the steady state period of 2002 to 2004. In the medium particles case, reentry alumina is evenly distributed across northern and southern latitudes and is the most abundant in the stratosphere, but persists in high mixing ratios above 40 km in the mesosphere. The small particles and averaged emissions cases show

Table 4: Global Direct Radiative Forcing (mW/m^2) for longwave and shortwave bands and the cumulative total radiative forcing over all wavelengths measured at the top of the atmosphere, the tropopause and surface for 2.52 Gg/yr flux. The Efficacy of Reentry Alumina ($mW/m^2/Tg$) based on the total radiative effect and the atmospheric burden is shown in parenthesis.

Test Case	Top of the Atmosphere			Tropopause			Surface		
	Long	Short	Total	Long	Short	Total	Long	Short	Total
Medium	0.0853	-0.492	-0.407 (-0.228)	0.0652	-0.599	-0.534 (-0.3)	0.0278	-0.458	-0.430 (-0.241)
Small	0.103	-0.549	-0.446 (-0.162)	0.0899	-0.709	-0.619 (-0.225)	0.0158	-0.588	-0.572 (-0.208)
Averaged	0.101	-0.596	-0.495 (-0.236)	0.0763	-0.732	-0.655 (-0.312)	0.0135	-0.535	-0.521 (-0.248)
South Pacific	0.0836	-0.489	-0.406 (-0.229)	0.0625	-0.607	-0.545 (-0.307)	0.0124	-0.455	-0.443 (-0.250)

similar distributions in their dominant modes. The small particles case shows a slight accumulation of reentry alumina in the mesosphere over the northern tropics.

The South Pacific case differs from the other cases. Here, reentry alumina accumulates strongly in the Southern hemisphere and at higher altitudes. Some reentry alumina does transition into the Northern hemisphere in the lower mesosphere and stratosphere. This result indicates that reentries localized in the South Pacific will lead to stronger particle accumulation in the Southern Hemisphere and will not diffuse across the entire atmosphere uniformly.

3.2 Direct Radiative Forcing

Table 4 shows the direct radiative forcing of reentry alumina at the top of the atmosphere, tropopause and Earth's surface for a reentry flux of 2.52 Gg. We compute these results using linear rescaling of our 1.33 Tg emission output. In parenthesis, we show the the direct radiative forcing efficacy, calculated per kilogram of steady state burden summed across all dust modes.

From Table 4, we can see that the cases with longer reentry alumina lifetimes have stronger direct radiative effects. Reentry alumina emissions with smaller particle sizes leads to approximately 16% larger direct radiative effect over larger particle sizes at the tropopause. However, the cases with high burdens of coarse mode particles are more effective at generating a direct radiative forcing. This result highlights the tradeoff between short-lived particles with large optical cross sections and long-lived particles with small optical cross sections. Balancing these trades, the averaged case with long-lived and large particles results in the second highest direct radiative effect, and the highest efficacy. In fact, the time-averaged representation of reentry emissions results in 22% overestimation of reentry alumina's direct radiative effect.

The South Pacific case, where reentry emissions occur only in the South Pacific, has a similar lifetime and global direct radiative forcing as the medium particles case, despite a clear difference in the reentry alumina distribution. To examine these results in more detail, Figure 4 shows the distribution of the direct radiative effect of reentry alumina at the top of the atmosphere for the medium particles and South Pacific case. From these distributions, we can see that South Pacific case has its strongest direct ra-

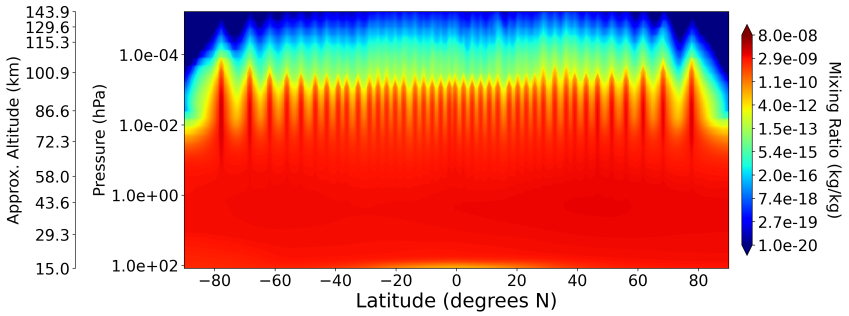

(a) Medium Particles Case, showing the burden of coarse mode particles

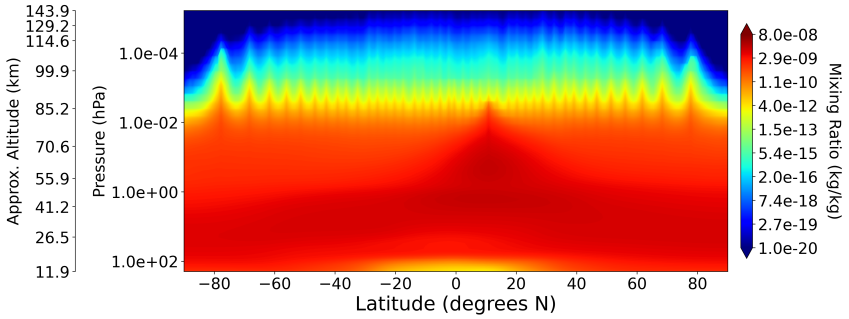

(b) Small Particles Case, showing the mass ratio of accumulation mode particles

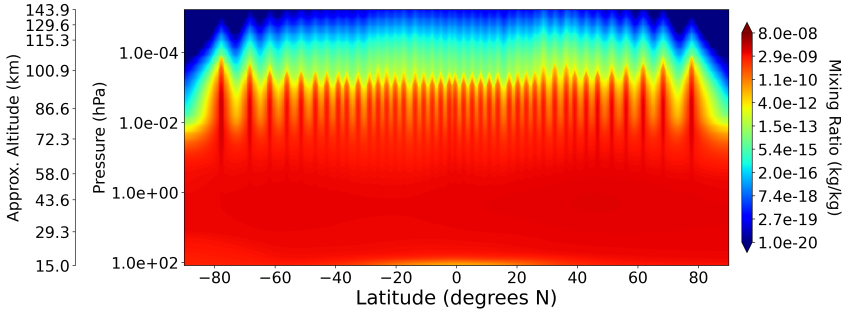

(c) Averaged Emissions Case, showing the mass ratio of coarse mode particles

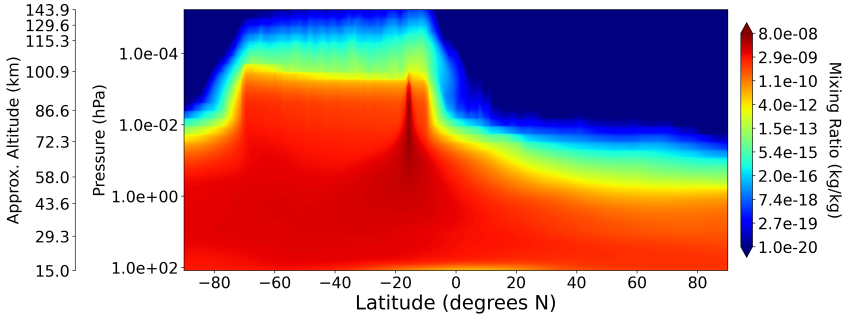

(d) South Pacific Case, showing the mass ratio of coarse mode particles

Figure 3: The mass ratio of the dominant particle mode to the air mass for each case. Each mass ratio is averaged over longitude at a given latitude and altitude.

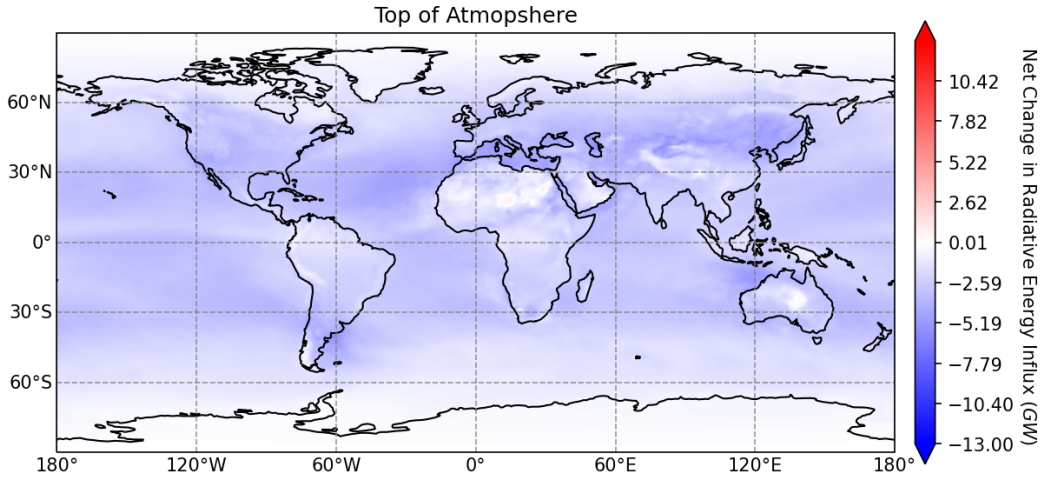

(a) Medium Particles Case

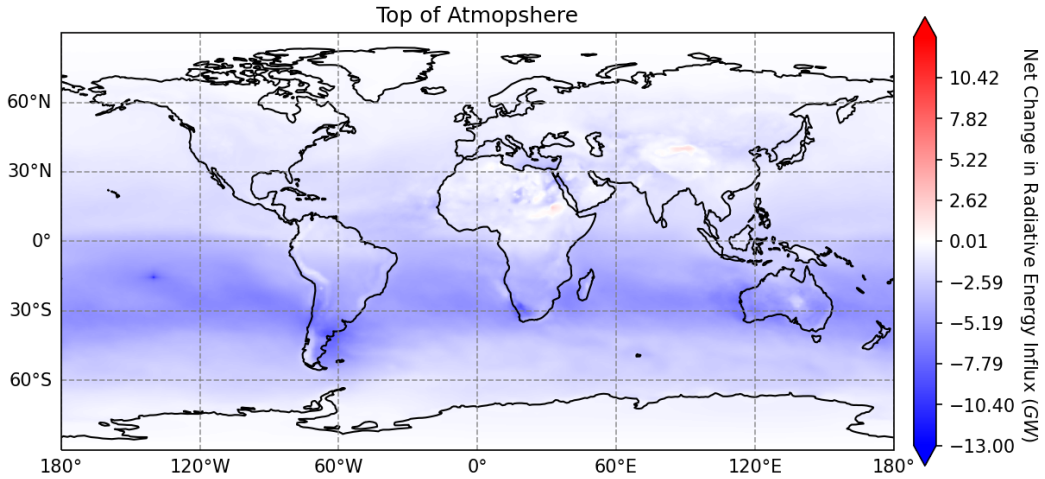

(b) South Pacific Case

Figure 4: Spatial distribution of the net change of radiative energy influx at the top of the atmosphere for the Medium Particles and South Pacific cases. Negative sign indicates less energy into Earth's surface.

diative effects in the South Pacific, unlike the medium particles case which shows nearly uniform radiative effects across the northern and southern mid-latitudes. Therefore, while the global direct radiative forcing is similar between the medium particles and South Pacific case, reentry alumina in the South Pacific case has direct radiative effects that disproportionately impact the South Pacific.

This kind of imbalance over the long-term could move the inter-tropical convergence zone (ITCZ), increase tropical cyclone activity and change to precipitation in many equatorial countries (Haywood et al., 2013; Cheng et al., 2022; Schneider et al., 2014). The degree to which the reentry alumina in the South Pacific case induces these secondary consequences was not captured in this study.

4 Discussion

4.1 Comparison with Aviation and Rockets

The net aviation radiative forcing (RF) is approximately 150 $mW/m^2 \pm 50$ mW/m^2 (Lee et al., 2021) measured at the tropopause. Aviation aerosol emissions have a direct radiative forcing of approximately 0.94 mW/m^2 while CO_2 emissions and contrails comprise a large fraction of aviation's positive radiative forcing (Lee et al., 2021). For context, aviation emissions have contributed approximately 4% to human-induced global warming (Klöwer et al., 2021).

This estimate of the net aviation RF was computed using aviation emissions since 1940 to 2018 to calculate the effects on 2018 conditions, adjusting for stratospheric heating (Lee et al., 2021). As a result, aviation's 150 mW/m^2 RF is based on transient, and not steady state, behavior with aviation emissions generally increasing year over year. In contrast, this work presents the instantaneous radiative forcing of reentries at steady state, corresponding to a hypothetical future scenario where megaconstellations achieve and maintain their designed size on orbit. Comparisons between aviation and this work's results are limited by these differences in methodologies, but provide a better understanding of the relative importance of reentry radiative forcing.

A future reentry scenario with 2.52 Gg/yr alumina flux produces approximately 0.33% to 0.43% of present-day aviation ERF. At a reentry flux of 1.33 Tg, 530 times larger than the estimated steady state flux from megconstellations, reentry-ablated alumina begins to produce a larger radiative effect than present-day aviation. This result indicates that even under a high-growth scenario with several megaconstellations in operation, the direct radiative effect of space debris reentries is small compared to aviation. Furthermore, the present-day space debris alumina reentry flux which is approximately 0.1-0.2 Gg (or less than 10% of this study's flux) is about four orders of magnitude smaller than aviation.

This comparison relies on aviation radiative forcing from 1940-2018 while the space debris reentry radiative effect corresponds to a 2050 reentry flux. By 2050, the net radiative effect of aviation may decrease given that the aviation industry is committed to reducing its climate impact (Mithal & Rutherford, 2023). Several organizations plan to reduce future carbon emissions by more than 50% compared to 2019 carbon emissions by 2050 (Mithal & Rutherford, 2023). If the aviation radiative forcing decreases, the ratio of reentry and aviation radiative forcing will increase.

Serving as another point for comparison, reentry-ablated alumina produces between 1% and 16% of direct radiative forcing of modern rocket fleets (Ross & Sheaffer, 2014; Ryan et al., 2022). Acknowledging caveats on poorly constrained alumina and black carbon optical properties, one study estimated global rocket launches in 2030 would produce a direct radiative forcing of 36 mW/m^2 (Ross & Sheaffer, 2014). Another study used the 2019 rocket fleet and applied an launch growth rate of 5.6% per year (Ryan et al., 2022). After a decade of growing rocket emissions, the direct radiative effect of this rocket fleet was 3.9 mW/m^2 (Ryan et al., 2022). This same study also explored a space tourism scenario with 400 Virgin Galactic suborbital flights per year, daily Blue Origin suborbital flights and weekly SpaceX launches (Ryan et al., 2022). In this case, the direct radiative effect of rockets of approximately 7.7 mW/m^2 (Ryan et al., 2022). This wide range of estimates for rocket radiative forcing reflects the uncertainty in future rocket emissions and launch rates.

With the projected growth of the space economy, the number of launches and reentries are likely to grow. These high-altitude emissions could be coupled, resulting in amplified atmospheric impacts. Studies of chlorine and alumina emissions from solid rocket motors have shown significant ozone depletion in the rocket plume due to $ClONO_2 + HCl \rightarrow Cl_2 + HNO_3$ heterogeneous reaction on alumina particles (Danilin et al., 2001;

Molina et al., 1997). Reentry alumina could increase the surface area available for this reaction among others. Furthermore, the warming effect of rocket emitted black carbon could be offset by the cooling effect of reentry ablated alumina, but cause local stratospheric temperature perturbations. These coupled effects should be explored in further work to gain a holistic insight on the impact of these emissions.

4.2 Caveats to Results

These results come with the caveats and limitations related to using dust as a proxy for alumina, as discussed in section 2.3. The coagulation characteristics from alumina particles generated from reentry ablation are not fully known. It is possible that dust coagulates more rapidly than alumina would otherwise. Faster coagulation would cause smaller particles to transition into larger particles more quickly which lowers an aerosol's atmospheric lifetime. If alumina coagulates slower than dust, we can expect the lifetimes of alumina particles to increase.

Furthermore, terrestrial dust is less effective at scattering light than alumina by approximately 10% to 20%. Therefore, the direct radiative forcing results may be underestimated. We also had to assume a linear relationship between the emission amount and direct radiative effect, which may not be true for a large scaling factor.

To bound the conservative nature of our results, we compare our findings with Weisenstein et al. (2015) which studied geoengineering with stratospheric alumina. We find our estimations for the shortwave radiative forcing in the small particle case per terragram emitted is approximately 25% smaller than the geoengineering finding for 640 nm alumina stratospheric particles at a 1Tg/yr flux (Weisenstein et al., 2015). In addition to dust being less effective at scattering than alumina, our study assumed alumina could coagulate efficiently, whereas Weisenstein et al. (2015) did not. This difference could also contribute to a lower estimation of shortwave radiative forcing.

Furthermore, we neglect to consider other sources of radiative forcing, such as NO_x emissions which interact with ozone chemistry and consequently, indirect changes to radiative transfer. This study also only evaluates one atmospheric impact, and neglects to consider other potential atmospheric interactions with reentry-ablated alumina, including high-altitude cloud formation, ozone depletion, ionospheric disruption and interactions with meteoric chemistry in the mesosphere. These interactions are necessary to study for a holistic understanding of the atmospheric effects of space debris reentry.

4.3 Future Work

As this work has shown, the characteristics of reentry-ablated alumina can alter the particle's lifetime and direct radiative effect. To reduce uncertainties in this model, future work should measure the particle size distribution of reentry-ablated alumina and characterize the optical and coagulation properties of these particles. Future studies can also improve upon the methodology presented in this work by implementing an alumina aerosol in a general circulation model, like WACCM. This new approach will improve estimations of the reentry radiative forcing for any desired reentry flux and can capture the coupled interactions between alumina's heterogeneous chemistry, cloud nucleation and indirect radiative forcing. Also, the deposition distribution of alumina can be modeled, allowing estimations of human and biota poisoning which has not yet been quantified (Herndon, 2015; Whiteside & Herndon, 2018). Furthermore, rocket and reentry emissions are likely coupled. Studying these feedbacks in future work would provide a better understanding of the atmospheric impact of launching satellites.

To validate results of this work and future modeling, in-situ sampling is vital. Atmospheric sampling through stratospheric planes, sounding rockets or weather balloons may be able to collect these particles and characterize their coagulation and size char-

acteristics. Alumina particles may also interact with meteoric metal chemistry in the mesosphere which may be possible to detect with ground lidar systems. Satellite observations may also be able to detect reentry particle accumulation or local ozone depletion. These observations will validate model results and likely improve our understanding of how alumina particles interact in the upper atmosphere.

5 Conclusion

This work presents results that characterize the distribution, lifetime and direct radiative effect of reentry-ablated alumina using a state-of-the-art general circulation model, WACCM. We explore a future scenario where all currently filed megaconstellations at the FCC are operating at full orbital capacity. In this scenario, we expect 14,400 reentry events per year with 13,900 satellites and 500 rocket bodies reentries, corresponding to an alumina influx of 2.52 Gg per year.

Our method uses terrestrial dust as a proxy for alumina. Dust can be represented in three modal particle size distributions, ranging from 0.1 μm to 10 μm, and can coagulate. Like alumina, dust scatters light but is less effective. Therefore, results presented in this work are conservative and assume alumina coagulates as efficiently as dust. If reentry-ablated alumina does not coagulate efficiently, the lifetimes of these particles will be underestimated in this work.

Several test cases are evaluated to identify the effect of various assumptions on particle size, emission location and the representation of reentry plumes as discrete events. In each case, we evaluate the steady state behavior with the reentry emissions repeating identically year-over-year.

Our results show that the lifetime and distribution of reentry-ablated alumina particles varies with different assumptions on the emitted particle size. Emissions modeled with discrete reentry plumes in the 0.01 to 0.1 μm particle size distribution result in the longest particle lifetime of 749 days. The same emitted mass in the 0.1 to 1 μm particle size distribution results in a shorter lifetime of 489 days. Subject to the assumptions in this methodology, these findings suggest that reentry alumina particles have a shorter lifetime than previous assumptions for rocket-produced alumina (Ross & Sheaffer, 2014).

Furthermore, we have shown that modeling reentry emissions with discrete reentry plumes results in shorter particle lifetimes than time-averaged emissions. Without modeling discrete plume emissions, the particle lifetimes will be overestimated by approximately 22%. Consequently, the extent to which these particles interact with atmospheric processes will also be overestimated using non-discrete representations of reentry plumes.

We also find that globally-emitted reentry particles are uniformly distributed across latitude in the mesosphere and stratosphere. These results suggest that reentry particles could alter other upper atmosphere and stratospheric processes, including ozone chemistry, high-altitude cloud nucleation, and meteoric chemistry.

Furthermore, this work has shown that reentry-ablated alumina produces a cooling instantaneous radiative forcing of approximately -200 mW/m^2 for a yearly reentry flux of 1.33 Tg which is 530 times larger than the optimistic megaconstellation scenario we considered. To compare, the aviation industry produces a total net radiative forcing of 100 mW/m^2, contributing approximately 4% to the global human-induce radiative forcing (Lee et al., 2021; Klöwer et al., 2021). With 2.52 Gg of reentry-ablated alumina, the estimated direct radiative forcing is -0.5 mW/m^2 to -0.65 mW/m^2 at the tropopause or 0.33% to 0.43% of aviation's radiative forcing.

From these results, we can conclude that the present-day and future flux of space debris reentries likely produces a small direct radiative forcing. We can also observe that optimizing satellite design for complete demise during reentry could increase the direct radiative effect of space debris reentries, but would not be sufficient to cause a radiative forcing comparable to the aviation industry. Therefore, this work supports designing for improved satellite demisability.

Our results show that consistent reentry into the South Pacific region produces a much higher concentration of alumina particles in the Southern Hemisphere than the Northern Hemisphere. This asymmetrical distribution of alumina resulted in an asymmetrical radiative effect that disproportionately effects the Southern Hemisphere. Asymmetrical radiative forcing can lead to severe climate consequences, including intense drought, and increased cyclone activity, at radiative forcing magnitudes greater than 1 W/m^2 (Haywood et al., 2013; Cheng et al., 2022; Schneider et al., 2014; Visioni et al., 2017). The extent to which reentries produce these negative climate impacts was not explored in this study. However, reentering space debris objects across the globe leads to more uniform radiative effects which limits the potential for these negative consequences. We can conclude that from a radiative forcing perspective, it may not be advantageous to implement policies that recommend or require all space debris objects to reenter over a singe region, such as the South Pacific.

Reentry-ablated alumina influx is likely to increase for the next several decades, given the rising number of orbiting objects, growing number of space actors and the development of mega-constellations. Beyond radiative forcing, these alumina particles may interact with several other important processes in the atmosphere and biosphere, including cloud nucleation, meteoric chemistry interactions, ozone depletion, vegetation poisoning, water contamination, and human health impacts (Herndon, 2015; Effiong & Neitzel, 2016). Further study, modeling and monitoring for these effects is necessary to understand the full scope of environmental consequences and determine reasonable metrics and thresholds for sustainable interactions with Earth's environment.

6 Open Research

This work relied on the Community Earth System Model (CESM) and the Whole Atmosphere Community Climate Model (WACCM) available at: `https://github.com/ESCOMP/CESM`.

Computing and data storage resources, including the Cheyenne supercomputer (doi:10.5065/D6RX99HX), were provided by the Computational and Information Systems Laboratory (CISL) at NCAR. NCAR is sponsored by the National Science Foundation.

Acknowledgments

Many thanks to Dr. Arlene Fiore and Dr. Jeffery Scott in the Department of Earth and Planetary Sciences at MIT for your support of this work. Thank you to Dr. Natalie Mahowald and Sarah Deutsch for sharing your expertise on dust modeling and modifying prognostic dust emissions. Thank you to Dr. Christopher Maloney your insight on modeling alumina aerosols. Thank you to Dr. Wuhu Feng and Dr. John Plane for sharing your expertise on meteoric atmospheric chemistry.

Thank you to Dr. Douglas Kinnison, Dr. Mike Mills, Dr. Francis Vitt, Dr. Simone Tilmes, Dr. Charles Bardeen, and Dr. Louisa Emmons for your expert guidance in selecting the appropriate component model. Furthermore, we thank all the scientists, software engineers, and administrators who contributed to the development of CESM2. The CESM project is supported primarily by the National Science Foundation.

References

Anwar, H. (2022, Jul). *New map pinpoints where starlink satellites re-enter earth's atmosphere for their disposal.* Retrieved from https://www.digitalinformationworld.com/2022/07/new-map-pinpoints-where-starlink.html

Beck, J. C., Holbrough, I., Schleutker, T., & Guelhan, A. (2019, Nov). Improved representation of destructive spacecraft re-entry from analysis of high enthalpy wind tunnel tests of spacecraft and equipment. *Acta Astronautica*, *164*, 287–296. Retrieved from https://linkinghub.elsevier.com/retrieve/pii/S0094576519312056 doi: 10.1016/j.actaastro.2019.07.033

Bekki, S., Beck, J., Lips, T., Merrifield, J., Spel, M., & Langener, T. (2021). *Environmental impacts of atmospheric emissions from spacecraft re-entry demise* [Project: ATmospheric Impact of SPAcecraft DEmise (ATISPADE)]. Retrieved from https://indico.esa.int/event/321/contributions/6403/attachments/4335/6538/esa-csid-21-bekki.pdf

Bianchi, S., Grassi, L., Yamashita, H., Dahlmann, K., Grewe, V., Jöckel, P., ... Laboulais, J. N. (2021). *Ara – atmoshperic re-entry assessment* [Thales Alenia Space]. Retrieved from https://indico.esa.int/event/321/contributions/6376/attachments/4334/6537/DESI_Bianchi_CleanSpaceIndustrialDays_ARA.pdf

Center for Orbital and Reentry Debris Studies. (2023). *Reentries.* The Aerospace Corporation. Retrieved from https://aerospace.org/reentries

Cheng, W., MacMartin, D. G., Kravitz, B., Visioni, D., Bednarz, E. M., Xu, Y., ... Deng, X. (2022, Apr). Changes in hadley circulation and intertropical convergence zone under strategic stratospheric aerosol geoengineering. *npj Climate and Atmospheric Science*, *5*(1), 32. Retrieved from https://www.nature.com/articles/s41612-022-00254-6 doi: 10.1038/s41612-022-00254-6

Chung, S. H. (2005). Climate response of direct radiative forcing of anthropogenic black carbon. *Journal of Geophysical Research*, *110*(D11), D11102. Retrieved from http://doi.wiley.com/10.1029/2004JD005441 doi: 10.1029/2004JD005441

Clough, S., Shephard, M., Mlawer, E., Delamere, J., Iacono, M., Cady-Pereira, K., ... Brown, P. (2005, Mar). Atmospheric radiative transfer modeling: a summary of the aer codes. *Journal of Quantitative Spectroscopy and Radiative Transfer*, *91*(2), 233–244. Retrieved from https://linkinghub.elsevier.com/retrieve/pii/S0022407304002158 doi: 10.1016/j.jqsrt.2004.05.058

Danilin, M., Shia, R.-L., Ko, M., Weisenstein, D., Sze, N., Lamb, J., ... Prather, M. (2001). Global stratospheric effects of the alumina emissions by solid-fueled rocket motors. *Journal of Geophysical Research: Atmospheres*, *106*(D12), 12727–12738.

De Lucia, V., & Iavicoli, V. (2019, Jun). From outer space to ocean depths: The 'spacecraft cemetery' and the protection of the marine environment in areas beyond national jurisdiction. *California Western International Law Journal*, *49*(2). Retrieved from https://scholarlycommons.law.cwsl.edu/cwilj/vol49/iss2/4

Effiong, U., & Neitzel, R. L. (2016, Dec). Assessing the direct occupational and public health impacts of solar radiation management with stratospheric aerosols. *Environmental Health*, *15*(1), 7, s12940-016-0089–0. Retrieved from http://ehjournal.biomedcentral.com/articles/10.1186/s12940-016-0089-0 doi: 10.1186/s12940-016-0089-0

European Space Agency. (2022a). *Esa's annual space environment report* (LOG No. GEN-DB-LOG-00288-OPS-SD). Retrieved from https://www.sdo.esoc.esa.int/environment_report/Space_Environment_Report_latest.pdf

European Space Agency. (2022b). *On the atmospheric impact of spacecraft demise upon reentry.* Retrieved from https://blogs.esa.int/cleanspace/2022/08/

11/on-the-atmospheric-impact-of-spacecraft-demise-upon-reentry/

Federal Communications Commission. (2022a, Sept). *Fcc adopts new "5-year rule" for deorbiting satellites to address growing risk of orbital debris.* 22-271 18-313. Retrieved from https://www.fcc.gov/document/fcc-adopts-new-5-year-rule-deorbiting-satellites

Federal Communications Commission. (2022b). *Space exploration holdings, llc, request for orbital deployment and operating authority for the spacex gen2 ngso satellite system* (Order Authorization No. FCC-22-91). Retrieved from https://www.fcc.gov/document/fcc-partially-grants-spacex-gen2-broadband-satellite-application

Fritz, T. M., Dedoussi, I. C., Eastham, S. D., Speth, R. L., Henze, D. K., & Barrett, S. R. (2022). Identifying the ozone-neutral aircraft cruise altitude. *Atmospheric Environment*, *276*, 119057.

Gettelman, A., Mills, M. J., Kinnison, D. E., Garcia, R. R., Smith, A. K., Marsh, D. R., ... Randel, W. J. (2019, Dec). The whole atmosphere community climate model version 6 (waccm6). *Journal of Geophysical Research: Atmospheres*, *124*(23), 12380–12403. Retrieved from https://onlinelibrary.wiley.com/doi/10.1029/2019JD030943 doi: 10.1029/2019JD030943

Greene, B. R., & Sanchez, C. M. (2019). Demisability of gfrp and cfrp components of reentering orbital debris: Phase i test results. In *Iaass conference ỳmaking safety happenỳ.*

Haywood, J. M., Jones, A., Bellouin, N., & Stephenson, D. (2013, Jul). Asymmetric forcing from stratospheric aerosols impacts sahelian rainfall. *Nature Climate Change*, *3*(7), 660–665. Retrieved from http://www.nature.com/articles/nclimate1857 doi: 10.1038/nclimate1857

Haywood, J. M., & Shine, K. P. (1995, Mar). The effect of anthropogenic sulfate and soot aerosol on the clear sky planetary radiation budget. *Geophysical Research Letters*, *22*(5), 603–606. Retrieved from http://doi.wiley.com/10.1029/95GL00075 doi: 10.1029/95GL00075

Herndon, J. M. (2015). Aluminum poisoning of humanity and earth's biota by clandestine geoengineering activity: implications for india. *Current Science*, *108*(12), 2173–2177. Retrieved from https://www.jstor.org/stable/24905652

Iacono, M. J., Delamere, J. S., Mlawer, E. J., Shephard, M. W., Clough, S. A., & Collins, W. D. (2008, Jul). Radiative forcing by long-lived greenhouse gases: Calculations with the aer radiative transfer models. *Journal of Geophysical Research*, *113*(D13), D13103. Retrieved from http://doi.wiley.com/10.1029/2008JD009944 doi: 10.1029/2008JD009944

Iacono, M. J., Mlawer, E. J., Clough, S. A., & Morcrette, J.-J. (2000, Jun). Impact of an improved longwave radiation model, rrtm, on the energy budget and thermodynamic properties of the ncar community climate model, ccm3. *Journal of Geophysical Research: Atmospheres*, *105*(D11), 14873–14890. Retrieved from http://doi.wiley.com/10.1029/2000JD900091 doi: 10.1029/2000JD900091

Jain, A., & Hastings, D. (2022, Sep). A model of space debris aluminum injection in the atmosphere. Paris, France: International Astronautical Federation (IAF).

Jo, D. S., Park, R. J., Jeong, J. I., Curci, G., Lee, H.-M., & Kim, S.-W. (2017). *Key factors affecting single scattering albedo calculation: Implications for aerosol climate forcing* [preprint]. Retrieved from https://acp.copernicus.org/preprints/acp-2017-1104/ doi: 10.5194/acp-2017-1104

Jones, K. L., Jain, A. K., & Cates, G. (2023, Mar). Green and circular space systems through environmental life cycle assessments. Austin, TX: STM 2023 Conference. Retrieved from https://web.tresorit.com/l/b2cgc#8T1h86yuZ2SdwScwfc_vtA&viewer=DcJLxyQkDlsgVsMPnHBrutChHI08AAZX

Ke, Z., Liu, X., Wu, M., Shan, Y., & Shi, Y. (2022, Jul). Improved dust rep-

resentation and impacts on dust transport and radiative effect in cam5. *Journal of Advances in Modeling Earth Systems*, *14*(7). Retrieved from https://onlinelibrary.wiley.com/doi/10.1029/2021MS002845 doi: 10.1029/2021MS002845

Kiehl, J. T., & Trenberth, K. E. (1997, Feb). Earth's annual global mean energy budget. *Bulletin of the American Meteorological Society*, *78*(2), 197–208. Retrieved from http://journals.ametsoc.org/doi/10.1175/1520-0477(1997)078<0197:EAGMEB>2.0.CO;2 doi: 10.1175/1520-0477(1997)078⟨0197:EAGMEB⟩2.0.CO;2

Klöwer, M., Allen, M. R., Lee, D. S., Proud, S. R., Gallagher, L., & Skowron, A. (2021, Oct). Quantifying aviation's contribution to global warming. *Environmental Research Letters*, *16*(10), 104027. Retrieved from https://iopscience.iop.org/article/10.1088/1748-9326/ac286e doi: 10.1088/1748-9326/ac286e

Lee, D., Fahey, D., Skowron, A., Allen, M., Burkhardt, U., Chen, Q., ... Wilcox, L. (2021, Jan). The contribution of global aviation to anthropogenic climate forcing for 2000 to 2018. *Atmospheric Environment*, *244*, 117834. Retrieved from https://linkinghub.elsevier.com/retrieve/pii/S1352231020305689 doi: 10.1016/j.atmosenv.2020.117834

Lips, T. (2003). Re-entry analysis of terrasar-x with scarab. In *54th international astronautical congress of the international astronautical federation, the international academy of astronautics, and the international institute of space law* (pp. IAA–5).

Liu, X. (2023, Mar). *Email Communication with Dr.Xiaohong Liu at the University of Texas at A&M.*

Liu, X., Easter, R. C., Ghan, S. J., Zaveri, R., Rasch, P., Shi, X., ... Mitchell, D. (2012, May). Toward a minimal representation of aerosols in climate models: description and evaluation in the community atmosphere model cam5, supplement document. *Geoscientific Model Development*, *5*(3), 709–739. Retrieved from https://gmd.copernicus.org/articles/5/709/2012/ doi: 10.5194/gmd-5-709-2012

Liu, X., Ma, P.-L., Wang, H., Tilmes, S., Singh, B., Easter, R. C., ... Rasch, P. J. (2016, Feb). Description and evaluation of a new four-mode version of the modal aerosol module (mam4) within version 5.3 of the community atmosphere model. *Geoscientific Model Development*, *9*(2), 505–522. Retrieved from https://gmd.copernicus.org/articles/9/505/2016/gmd-9-505-2016.html doi: 10.5194/gmd-9-505-2016

Liu, X., Penner, J. E., & Herzog, M. (2005). Global modeling of aerosol dynamics: Model description, evaluation, and interactions between sulfate and nonsulfate aerosols. *Journal of Geophysical Research: Atmospheres*, *110*(D18).

Marsh, D. R., Mills, M. J., Kinnison, D. E., Lamarque, J.-F., Calvo, N., & Polvani, L. M. (2013, Oct). Climate change from 1850 to 2005 simulated in cesm1(waccm). *Journal of Climate*, *26*(19), 7372–7391. Retrieved from https://journals.ametsoc.org/view/journals/clim/26/19/jcli-d-12-00558.1.xml doi: 10.1175/JCLI-D-12-00558.1

Miller, R. L., Tegen, I., & Perlwitz, J. (2004, Feb). Surface radiative forcing by soil dust aerosols and the hydrologic cycle: Dust forcing and the hydrologic cycle. *Journal of Geophysical Research: Atmospheres*, *109*(D4), n/a-n/a. Retrieved from http://doi.wiley.com/10.1029/2003JD004085 doi: 10.1029/2003JD004085

Mills, M. (2022). *Input data for grids.* Retrieved from ftp://nitrogen.acom.ucar.edu/user/mmills/inputdata/grids

Mithal, S., & Rutherford, D. (2023, Jan). *Icao's 2050 net-zero co2 goal for international aviation.* THE INTERNATIONAL COUNCIL ON CLEAN TRANSPORTATION. Retrieved from https://theicct.org/publication/global

-aviation-icao-net-zero-goal-jan23/

Mlawer, E. J., Taubman, S. J., Brown, P. D., Iacono, M. J., & Clough, S. A. (1997, Jul). Radiative transfer for inhomogeneous atmospheres: Rrtm, a validated correlated-k model for the longwave. *Journal of Geophysical Research: Atmospheres*, *102*(D14), 16663–16682. Retrieved from http://doi.wiley.com/10.1029/97JD00237 doi: 10.1029/97JD00237

Molina, M. J., Molina, L. T., Zhang, R., Meads, R. F., & Spencer, D. D. (1997, Jul). The reaction of clono 2 with hcl on aluminum oxide. *Geophysical Research Letters*, *24*(13), 1619–1622. Retrieved from http://doi.wiley.com/10.1029/97GL01560 doi: 10.1029/97gl01560

Palik, E. D. (1985). *Handbook of optical constants of solids*. Orlando San Diego New York: Academic press.

Pardini, C., & Anselmo, L. (2008). Impact of the time span selected to calibrate the ballistic parameter on spacecraft re-entry predictions. *Advances in Space Research*, *41*(7), 1100–1114.

Park, S.-H., & Park, G. (2017, Sep). Reentry trajectory and survivability estimation of small space debris with catalytic recombination. *Advances in Space Research*, *60*(5), 893–906. Retrieved from https://linkinghub.elsevier.com/retrieve/pii/S0273117717303332 doi: 10.1016/j.asr.2017.05.004

Plane, J. M. C., Daly, S. M., Feng, W., Gerding, M., & Gómez Martín, J. C. (2021, Feb). Meteor-ablated aluminum in the mesosphere-lower thermosphere. *Journal of Geophysical Research: Space Physics*, *126*(2). Retrieved from https://onlinelibrary.wiley.com/doi/10.1029/2020JA028792 doi: 10.1029/2020JA028792

Plane, J. M. C., Feng, W., & Dawkins, E. C. M. (2015, May). The mesosphere and metals: Chemistry and changes. *Chemical Reviews*, *115*(10), 4497–4541. doi: 10.1021/cr500501m

Rainbow, J. (2022, Feb). *Wyler raises $50 million for "sustainable" megaconstellation.* Retrieved from https://spacenews.com/wyler-raises-50-million-for-sustainable-megaconstellation/

Ross, M. N., & Sheaffer, P. M. (2014, Apr). Radiative forcing caused by rocket engine emissions. *Earth's Future*, *2*(4), 177–196. doi: 10.1002/2013ef000160

Ryan, R. G., Marais, E. A., Balhatchet, C. J., & Eastham, S. D. (2022). *Impact of rocket launch and space debris air pollutant emissions on stratospheric ozone and global climate.* Retrieved from http://www.essoar.org/doi/10.1002/essoar.10510460.1 doi: 10.1002/essoar.10510460.1

Ryan-Mosley, T., Winick, E., & Kakaes, K. (2019, Jun). The number of satellites orbiting earth could quintuple in the next decade. *MIT Technology Review*. Retrieved from https://www.technologyreview.com/2019/06/26/755/satellite-constellations-orbiting-earth-quintuple/

Schneider, T., Bischoff, T., & Haug, G. H. (2014, Sep). Migrations and dynamics of the intertropical convergence zone. *Nature*, *513*(7516), 45–53. Retrieved from http://www.nature.com/articles/nature13636 doi: 10.1038/nature13636

Schulz, L., & Glassmeier, K.-H. (2021, Feb). On the anthropogenic and natural injection of matter into earth's atmosphere. *Advances in Space Research*, *67*(3), 1002–1025. Retrieved from https://linkinghub.elsevier.com/retrieve/pii/S0273117720307663 doi: 10.1016/j.asr.2020.10.036

Smith, K. L., Neely, R. R., Marsh, D. R., & Polvani, L. M. (2014, Sep). The specified chemistry whole atmosphere community climate model (sc-waccm). *Journal of Advances in Modeling Earth Systems*, *6*(3), 883–901. Retrieved from http://doi.wiley.com/10.1002/2014MS000346 doi: 10.1002/2014MS000346

Tilmes, S., Mills, M. J., Zhu, Y., Bardeen, C. G., Vitt, F., Yu, P., ... Deshler, T. (2023). *Description and performance of the carma sectional aerosol microphysical model in cesm2* [preprint]. Retrieved from https://gmd.copernicus.org/

preprints/gmd-2023-79/ doi: 10.5194/gmd-2023-79

United Nations. (2019, Feb). *Compendium: Space debris mitigation standards adopted by states and international organizations.* Retrieved from https://www.unoosa.org/documents/pdf/spacelaw/sd/Space_Debris_Compendium_COPUOS_25_Feb_2019p.pdf

US EPA, OAR. (2017, Jun). *Basic ozone layer science* [Reports and Assessments]. Retrieved from https://www.epa.gov/ozone-layer-protection/basic-ozone-layer-science

Visioni, D., Pitari, G., & Aquila, V. (2017, Mar). Sulfate geoengineering: a review of the factors controlling the needed injection of sulfur dioxide. *Atmospheric Chemistry and Physics*, *17*(6), 3879–3889. Retrieved from https://acp.copernicus.org/articles/17/3879/2017/ doi: 10.5194/acp-17-3879-2017

Waugh, D., & Hall, T. (2002). Age of stratospheric air: Theory, observations, and models. *Reviews of Geophysics*, *40*(4), 1–1.

Weisenstein, D. K., Keith, D. W., & Dykema, J. A. (2015, Oct). Solar geoengineering using solid aerosol in the stratosphere. *Atmospheric Chemistry and Physics*, *15*(20), 11835–11859. Retrieved from https://acp.copernicus.org/articles/15/11835/2015/ doi: 10.5194/acp-15-11835-2015

Whiteside, M., & Herndon, J. M. (2018, Aug). Previously unacknowledged potential factors in catastrophic bee and insect die-off arising from coal fly ash geoengineering. *Asian Journal of Biology*, *6*(4), 1–13. Retrieved from https://journalajob.com/index.php/AJOB/article/view/16 doi: 10.9734/ajob/2018/43268

Wilcox, L., Shine, K., & Hoskins, B. (2012). Radiative forcing due to aviation water vapour emissions. *Atmospheric Environment*, *63*, 1–13.

Williams, A., Hainaut, O., Otarola, A., Tan, G. H., & Rotola, G. (2021). Analysing the impact of satellite constellations and eso's role in supporting the astronomy community. *Published in The Messenger vol. 184, pp. 3-7*, 5 pages. Retrieved from http://doi.eso.org/10.18727/0722-6691/5237 doi: 10.18727/0722-6691/5237

Zhang, J., Wuebbles, D., Kinnison, D., & Baughcum, S. L. (2021, Aug). Stratospheric ozone and climate forcing sensitivity to cruise altitudes for fleets of potential supersonic transport aircraft. *Journal of Geophysical Research: Atmospheres*, *126*(16). Retrieved from https://onlinelibrary.wiley.com/doi/10.1029/2021JD034971 doi: 10.1029/2021JD034971

Ziniu, W., Ruifeng, H., Xi, Q., Xiang, W., & Zhe, W. (2011). Space debris reentry analysis methods and tools. *Chinese Journal of Aeronautics*, *24*(4), 387–395.